Journal of Biomedical Optics

SPIEDigitalLibrary.org/jbo

Rapid diagnosis of liver fibrosis using multimodal multiphoton nonlinear optical microspectroscopy imaging

Jang Hyuk Lee
Jong Chul Kim
Giyoong Tae
Myoung-kyu Oh
Do-Kyeong Ko

SPIE

Rapid diagnosis of liver fibrosis using multimodal multiphoton nonlinear optical microspectroscopy imaging

Jang Hyuk Lee,[a] Jong Chul Kim,[b] Giyoong Tae,[b] Myoung-kyu Oh,[c] and Do-Kyeong Ko[a]
[a]Gwangju Institute of Science and Technology, Department of Physics and Photon Science, Gwangju 500-712, Republic of Korea
[b]School of Materials Science and Engineering, Gwangju Institute of Science and Technology, Department of Nanobio Materials and Electronics, Gwangju 500-712, Republic of Korea
[c]Gwangju Institute of Science and Technology, Advanced Photonics Research Institute, Gwangju 500-712, Republic of Korea

Abstract. A multimodal multiphoton nonlinear optical (NLO) microspectroscopy imaging system was developed using a femtosecond laser and a photonic crystal fiber. Coherent anti-Stokes Raman scattering (CARS) microspectroscopy was combined with two-photon excitation fluorescence and second-harmonic generation microscopy in one platform and the system was applied to diagnose liver fibrosis. Normal and liver fibrosis tissues were clearly distinguished with the great difference from CARS spectra as well as multimodal multiphoton NLO images. We expect the system to be a rapid diagnosis tool for liver fibrosis at tissue level with label-free imaging of significant biochemical components. [DOI: 10.1117/1.JBO.18.7.076009]

Keywords: multiphoton nonlinear optical microscopy; coherent anti-Stokes Raman scattering microscopy; CARS spectroscopy; liver fibrosis.

Paper 130160RR received Mar. 20, 2013; revised manuscript received Jun. 6, 2013; accepted for publication Jun. 7, 2013; published online Jul. 9, 2013.

1 Introduction

Chronic liver disease is a major global health issue, and liver cancer is among the top 10 leading causes of death around the world.[1] Furthermore, liver disease is one of the top five leading causes of death in middle age in many developed countries.[2] Liver fibrosis is characterized by the excessive accumulation of extracellular matrix proteins including collagen, which occurs in most types of chronic liver diseases.[2] Cirrhosis, liver failure, liver cancer, and portal hypertension result from advanced liver fibrosis, and liver transplantation is frequently required. Therefore, chronic liver diseases are considered an important public health problem, and having a reliable diagnosis and early detection of fibrosis is important.

At present, liver biopsy is the clinical gold standard for assessing liver fibrosis.[3] However, the traditional method is costly, time-consuming, and laborious in the specimen preparation procedure that requires sample dehydration, fixation, slicing, and labeling. These limitations make liver biopsy inappropriate for diagnosis and longitudinal monitoring at the population level. Currently, several techniques are employed for liver fibrosis diagnosis, such as computed tomography and ultrasonography, even though they have the limitations of low spatial resolution, low sensitivity, and specificity. Therefore, the development of a fast, accurate, and reproducible test for diagnosis and monitoring of liver fibrosis is enormously valuable.

Significant advances for nondestructive characterization of intact biological tissues in their native conditions have been a result of the development of multiphoton optical microscopy. Especially, the two techniques of two-photon excited fluorescence (TPEF) and second-harmonic generation (SHG) microscopy are most widely employed for biomedical applications.[4] Multiphoton microscopy includes a lot of strengths such as three-dimensional optical sectioning, subcellular spatial resolution, deep penetration of thick specimens, and minimum destruction of samples as compared with the traditional histological examination.[5] TPEF signals are generated from the intrinsic molecules in liver tissue such as fiber elastin, nicotinamide adenine dinucleotide (NADH)/nicotinamide adenine dinucleotide phosphate (NADPH), and flavin adenine dinucleotide (FAD) with emitting intense fluorescence under excitation.[6] These molecules involved in cellular metabolism make TPEF microscopy suitable for image tissue morphologies.[7] SHG microscopy has been utilized to examine collagen fibrils in tissue since it is sensitive to the noncentrosymmetric microstructures.[8]

Coherent anti-Stokes Raman scattering (CARS) microscopy, which is another nonlinear multiphoton microscopy technique, has developed into a valuable label-free technique for biomedical imaging with high vibrational selectivity and sensitivity.[9,10] Since signals of CARS imaging are intrinsic and specific to particular molecular vibration such as aliphatic C-H bonds of lipids, it possesses chemical contrast without any requirement of employing exogenous labeling.[11]

As each nonlinear imaging modality has the differences in contrast mechanisms and biomolecular origins, combining those several multiphoton microscopies in one platform would be feasible for the observation of the composition of various biomolecules at tissue level.[12] The multimodal multiphoton nonlinear optical (NLO) microscopy imaging system would provide high sensitivity and specificity with rapid acquisition as a powerful tool for early stage detection of disease.

Recently, several research studies in the field of liver fibrosis and liver disease have been performed by using a multiphoton NLO microscopy, based on two tightly synchronized Ti:sapphire lasers. Brackmann et al. demonstrated clear differences

Address all correspondence to: Do-Kyeong Ko, Gwangju Institute of Science and Technology, Department of Physics and Photon Science, Gwangju 500-712, Republic of Korea. Tel: +82-62-715-2227; Fax : +82-62-715-2224; E-mail: dkko@gist.ac.kr

in lipid content and collagen fiber development by combining CARS and SHG microscopy.[13] They also indicated non-alcoholic fatty liver disease and steatohepatitis caused at a relatively early stage by Western diet. Lin et al. developed an integrated multiphoton microscopy imaging technique for monitoring the change of biochemical and biomolecular constituents and the structure of liver tissue, which is associated with the progression of liver steatosis and fibrosis induced in a bile duct ligation rat liver model.[14] However, the above-mentioned researches have several limitations such as their bulky laser systems and offering no chemical information of the sample.

In this paper, we demonstrated an integrated multiphoton NLO microspectroscopy imaging system, combining TPEF, SHG, and CARS microscopy in one platform, by using a single femtosecond oscillator along with photonic crystal fiber (PCF). In this system, we could obtain chemical constituents of a sample from the CARS spectra. From the multimodal images and CARS spectra of liver fibrosis tissue and normal liver tissue, we observed the changes of lipids, elastin, and collagen in the fibrosis tissue.

2 Experimental Setup and Methods

2.1 *Multimodal Multiphoton NLO Microspectroscopy Imaging System*

Figure 1 shows the schematic of our PCF-based multimodal multiphoton NLO microspectroscopy imaging system. This microspectroscopy imaging modality was modified and developed from a previously described system.[15,16] An LD-pumped green laser (Verdi V5, Coherent) was used as the pumping source of a home-made Ti:sapphire femtosecond oscillator. In this system, the output wavelength was centered at 800 nm with pulse duration of 60 fs, repetition rate of 56.1 MHz, and average output power of 460 mW. Figure 2(a) shows the spectral profile of laser oscillator, and the bandwidth of beams generated from oscillator is about 4 nm (full width half maximum). Figure 2(b) shows the measured pulse width of laser oscillator by autocorrelator, and the laser pulse duration is 60 fs with assuming Gaussian intensity profile. The femtosecond pulses passed through an optical isolator (IO-5-NIR-LP, Thorlabs, New Jersey), and the output power was divided into two beams (3:1) using a beam splitter (BP133, Thorlabs). The reflected beam was then transmitted through a series of optical components for spatial filtering, and narrow band "pump pulses" in CARS process, the pulse of 0.8 nm with the center wavelength 800 nm, was generated by combining two filters (LL01-808-12.5 and custom made filter by Semrock). Figure 2(c) shows the spectrum of our narrowband pump beam. In contrast, the transmitted pulse was coupled into the PCF (FemtoWHITE 800, NKT Photonics, Denmark) through an objective lens in order to make ultrabroadband "Stokes pulses." Figure 2(d) shows the measured spectrum of Stokes beam. The narrowband pump and broadband Stokes pulses were spatially and temporally overlapped using a long wavelength pass filter (BLP01-785R-25, Semrock, Illinois), and the two beams were passed through galvanometric mirrors. The collinear beams were tightly focused into the sample using an objective lens (LU Plan Fluor, 0.9 NA, 100×, Nikon, Japan), and forward nonlinear signals were collected by a condenser lens (0.4 NA, 20×, Olympus, Japan). The sample was mounted on an xy-axis piezo translation stage (SLC-1730, SmarAct, Germany), and its z-axis was controlled by a piezoelectric objective lens positioning system (Mipos100, Piezosystemjena, Germany). After the nonlinear signals passed through a short pass filter (FF01-775/SP-25, Semrock), the CARS spectrum signal was detected using a monochromator (DongWoo i500) and then recorded using a charge-coupled device camera (iDus, Newton) having an effective spectral resolution of 5 cm^{-1}.

To obtain multimodal nonlinear images, signals of CARS, TPEF, and SHG were spectrally separated by using dichroic mirrors and band pass filters (CARS: HQ650/20m, Chroma, TPEF: FF01-550/88, SHG: FF01-390/18, Semrock), and all their signals were simultaneously recorded by using two different photomultiplier tubes, one for CARS and the other for TPEF and SHG (H-8249-102, H-7827-012, Hamamatsu). The signals were converted to NLO images through a data acquisition program written in Labview 8.6. Typically, powers of 20 mW for the pump and 2 mW for Stokes pulses were used at the sample for imaging.

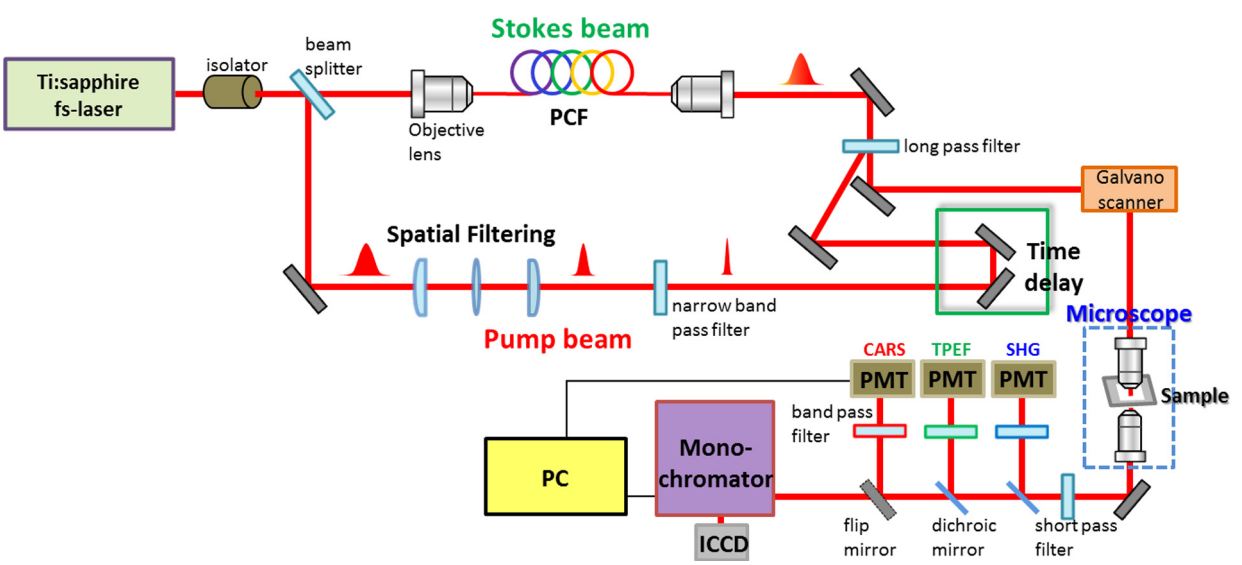

Fig. 1 Schematic of the multiphoton nonlinear optical (NLO) microspectroscopy imaging system.

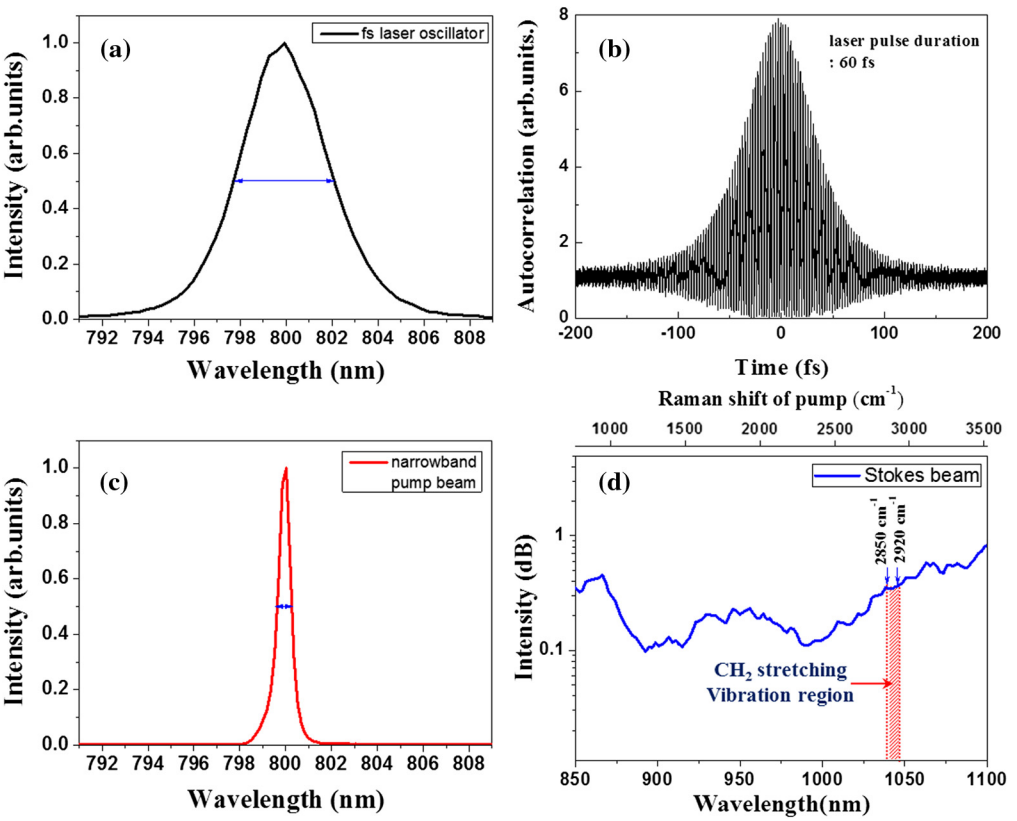

Fig. 2 (a) Spectral profile of femtosecond laser oscillator. (b) Measured pulse width of laser oscillator. (c) Spectrum of narrowband pump beam. (d) Spectrum of Stokes beam.

2.2 *Liver Tissue Preparation*

For sample preparation, BALB/c female mice weighing 20–25 g (8 weeks of age) were purchased from Orient-Bio (Gyeonggi-do, Korea). All of the animals were provided humane care with free access to feed and water. Hepatic fibrosis was induced by intraperitoneal injections of Thioacetamide (Sigma–Aldrich, USA) in dosages of 200 mg/kg, three times per week for 11 weeks.[17] After 4 weeks from the last injection, the mice were sacrificed, and their liver tissues were harvested. Liver tissues were embedded in optimum cutting temperature (OCT, Sakura Finetek Japan, Japan) compound to use a cryostat microtome (Leica CM1850, Wetzlar, Germany). The embedded liver tissues were frozen in a deep freezer for 30 min, and were sectioned into 8 μm thickness. OCT compound in tissue section was removed in water before analysis. CARS spectrum measurements were performed using tissue samples sectioned into 25 from the total eight mice for four normal and fibrosis.

2.3 *Histopathological Method*

To obtain a histopathological image, the fibrosis liver tissue was fixed in formalin solution and embedded in paraffin. Tissue sections were cut with 4 μm thickness, and one of the serial sections was stained with Gomori's trichrome staining.[18] Chromotrope-fast green solution of trichrome stain was used to stain collagen green and cytoplasm red. The unstained adjacent serial tissue section of trichrome stained slide was used to obtain multimodal nonlinear images.

3 Experimental Results

As we mentioned in the previous section, we have performed the experiment with 25 normal and 25 fibrosis samples each day and repeated four times, which means we measured 200 spectra in total. Figure 3 shows the comparison of typical CARS spectra between representative normal (top, blue line) and liver fibrosis tissue (bottom, red line) for four groups. The CARS spectrum was measured in the vicinity of aliphatic C-H stretching vibration mode and was obtained at an arbitrary point of lipid inside the tissue, not by the integration of the whole area of the tissue. Each point in normal and liver fibrosis groups had the same pattern of spectrum group by group besides the height of the intensity. The exposure time for taking a CARS spectrum was 0.1 s. As shown in the figure, regardless of the samples, all the spectra are quite similar for each of normal and fibrosis samples.

We chosed a pair of CARS spectra of normal and liver fibrosis and overlapped them as shown in Fig. 4(a). The spectra of normal and liver fibrosis are shown in blue line and red line, respectively. In normal liver tissue, two peaks with almost the same height were observed at 2850 and 2920 cm^{-1}, which correspond to CH_2 symmetry stretching vibration and CH_2 asymmetry stretching vibration, respectively. On the other hand, in liver fibrosis, CH_2 symmetry stretching vibration mode was strong but CH_2 asymmetry stretching vibration mode was clearly weakened. And olefinic=CH stretching vibration at 3150 cm^{-1} was equally observed in both samples.

In order to analyze the difference of CARS spectra between normal and liver fibrosis, all data were normalized by setting the peak of 2850 cm^{-1} equal to 1.0. Figure 4(b) shows the

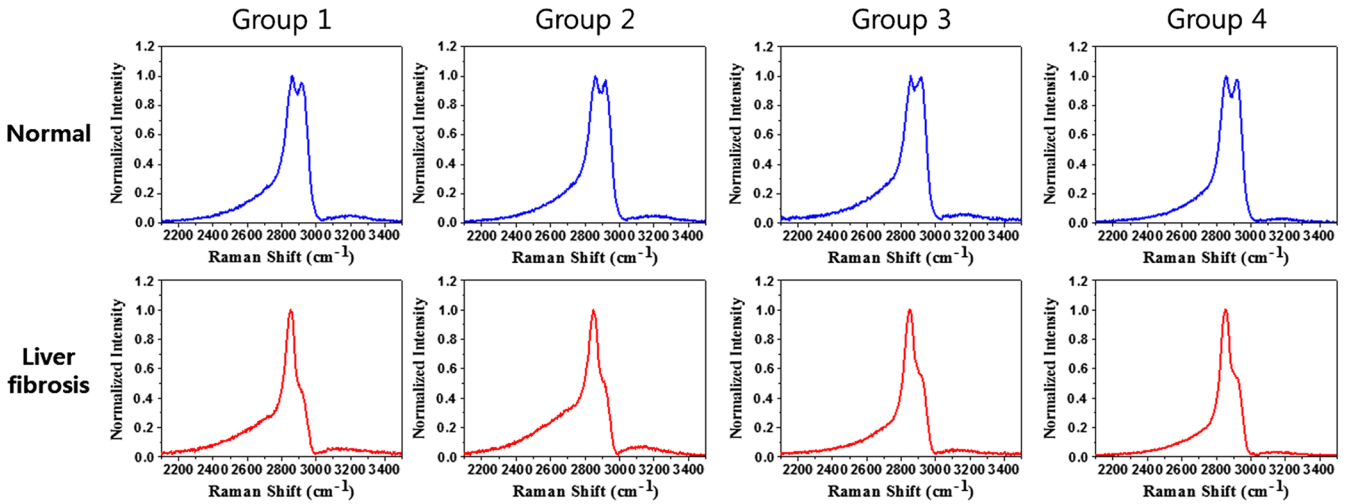

Fig. 3 Comparison of CARS spectra between representative normal (top, blue line) and liver fibrosis tissue (bottom, red line) for each group.

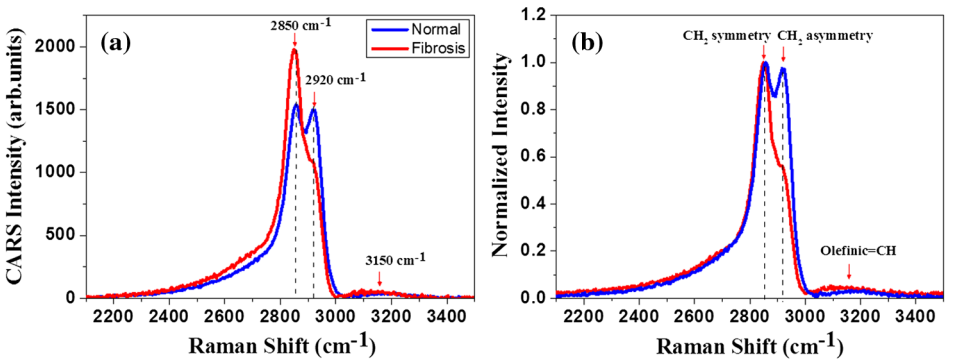

Fig. 4 (a) Comparison of typical CARS spectra between normal (blue line) and liver fibrosis tissue (red line) at CF038H stretching vibration. (b) Normalized CARS spectra of Fig. 4(a).

Table 1 The average and standard deviation of I_{2850}/I_{2920} between normal and liver fibrosis tissue.

	Normal		Liver fibrosis		
I_{2850}/I_{2920}	Average	Standard deviation	Average	Standard deviation	Ratio
Group 1	1.02	0.04	1.96	0.18	~1:1.92
Group 2	1.12	0.05	2.00	0.17	~1:1.79
Group 3	0.91	0.02	1.93	0.15	~1:2.12
Group 4	0.97	0.04	2.04	0.18	~1:2.10
Total average	1.00		1.98		~1:1.98

normalization of spectra from Fig. 4(a). For normalized CARS spectra from 100 normal and liver fibrosis samples, respectively, 2850 cm^{-1} peak intensity I_{2850} was divided by 2920 cm^{-1} peak intensity I_{2920}. Table 1 shows the average and standard deviation of the values I_{2850}/I_{2920} for each group. As a result, the ratio of the values I_{2850}/I_{2920} for normal to liver fibrosis is ~2:1, which means that CH_2 asymmetry stretching is suppressed in liver fibrosis. We speculate that it is due to changes in the structure and formation of lipid during the process of lipid peroxidation, which is implicated as a cause of liver fibrosis.[19]

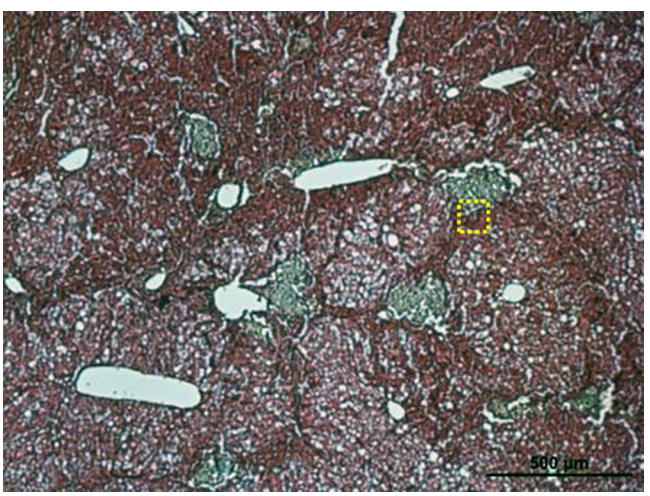

Fig. 5 Histopathological image of liver fibrosis tissue with Gomori's trichrome staining. Green color represents collagen in liver and red color shows cytoplasm.

Figure 5 shows the obtained histopathological image. Green color represents collagen in liver and red color shows cytoplasm. In addition, the region indicated by the yellow square in Fig. 5

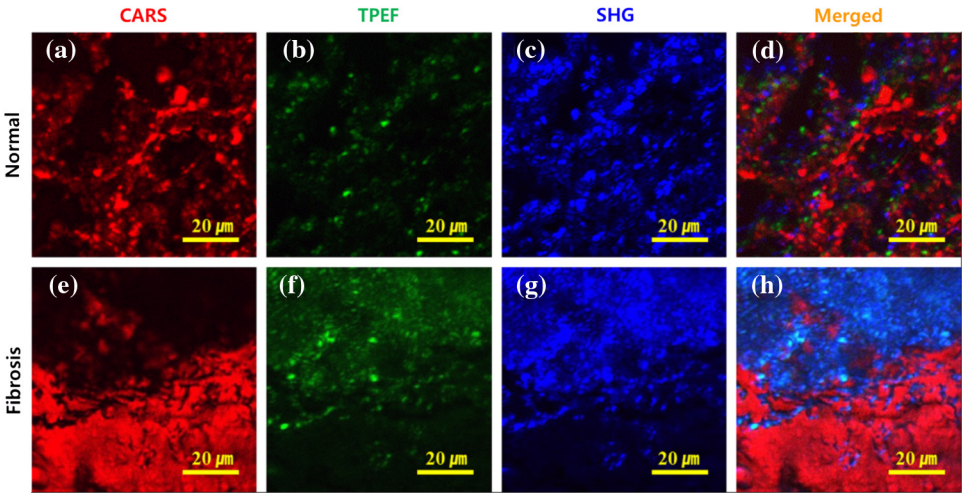

Fig. 6 Comparison of typical multimodal multiphoton NLO microscopy images between the normal (top) and liver fibrosis tissues (bottom). CARS images in (a) and (e), TPEF images in (b) and (f), SHG images (c) and (g), and merged images in (d) and (h). Red: CARS (lipid rich structure). Green: TPEF (elastin or other fluorescent particles). Blue: SHG (collagen). Scale bar is 20 μm.

was measured by using our multimodal NLO microspectroscopy imaging system. CARS, TPEF, and SHG were obtained simultaneously as shown in Fig. 6(e)–6(g), and the merging image of CARS, TPEF, and SHG is shown in Fig. 6(h). As a result, spot of the liver section showing clear boundary between collagen fibers and normal tissue from trichrome staining was imaged using multimodal multiphoton NLO microscopy.

In Fig. 6, we compared the observed multimodal multiphoton NLO microscopy (CARS/TPEF/SHG) images between the normal (top) and liver fibrosis tissues (bottom) from the same position of each sample at the same time. Each image was 80×80 μm^2 (300×300 pixels), the acquisition time per an image was within 5 s, and the size of scale bar was 20 μm. Figure 6(a) and 6(e) is the CARS images of normal and liver fibrosis obtained with above-mentioned resonant CARS signals of aliphatic C—H stretching vibration mode region. In normal tissue, we observed well-distributed CARS signal but, in fibrosing tissue, there was no signal in some areas [black color in Fig. 6(e)] and big signal outside the area. We think it is because collagen is accumulated during the fibrosis process and formed a mass in some areas and the lipid droplets are gathered outside the collagen-accumulated area. It is reported that collagen is produced during liver fibrosis.[2] Figure 6(b) and 6(f) shows the TPEF images of normal and liver fibrosis tissue, and it allows one to observe hepatocyte morphology and elastin by TPEF signals arising from NAD(P)H and flavins' autofluorescence in liver tissue. It is reported that the number of elastic fibers increases in fibrosis compared to the number of normal liver and our results support their result.[20] Figure 6(c) and 6(g) is SHG images of normal and liver fibrosis for observing changes of collagen. While very weak SHG signals of collagen were detected in normal liver tissue, very strong SHG signals were observed by the aggregated collagen in liver fibrosis, which confirmed the previous CARS image data.

The merged images (CARS, TPEF, and SHG) of normal and liver fibrosis tissues are shown in Fig. 6(d) and 6(h), respectively, which shows the changes of lipids, elastin, and collagen inside fibrosis tissue compared with the normal tissue. From the figures, we could see that few collagens and hepatic lipid droplets were observed in normal tissue and a lot of aggregated collagen fibers and hepatic lipid droplets were clearly visualized in liver fibrosis tissue, respectively.

4 Conclusion

In this paper, we have developed PCF-based multimodal multiphoton NLO microspectroscopy imaging system and applied it to normal and liver fibrosis tissue. The multimodal multiphoton NLO images provide distinct molecular structures and compositions (lipids, fiber elastin, and collagen) of liver tissue associated with fibrosis transformation. Furthermore, normal and liver fibrosis tissues were clearly distinguished by the great difference from CARS spectra with high spectral resolution through using narrowband pump beam. Besides, the multimodal multiphoton NLO microspectroscopy imaging system is time-saving and highly accurate compared to traditional histology techniques. Therefore, we expect the system to have potential value as a rapid diagnosis tool for liver fibrosis of tissue and label-free imaging of significant biochemical components as well.

Acknowledgments

This paper was supported by the National Research Foundation of Korea (NRF) grants funded by the Ministry of Science, ICT & Future Planning (2011-0015520, 2008-0062606, and 2011-0020956) and by grants from the Bio Imaging Research Center at GIST.

References

1. American Cancer Society, *Cancer Facts & Figures 2013*. American Cancer Society, Atlanta, GA (2013).
2. R. Bataller and D. A. Brenner, "Liver fibrosis," *J. Clin. Invest.* **115**(2), 209–218 (2005).
3. N. H. Afdhal and D. Nunes, "Evaluation of liver fibrosis: a concise review," *Am. J. Gastroenterol.* **99**(6), 1160–1174 (2004).
4. Y. Wu and J. Y. Qu, "Two-photon autofluorescence spectroscopy and second-harmonic generation of epithelial tissue," *Opt. Lett.* **30**(22), 3045–3047 (2005).
5. T. T. Le et al., "Label-free molecular imaging of atherosclerotic lesions using multimodal nonlinear optical microscopy," *J. Biomed. Opt.* **12**(5), 054007 (2007).

6. A. Pellicoro et al., "Elastin accumulation is regulated at the level of degradation by macrophage metalloelastase (MMP-12) during experimental liver fibrosis," *Hepatology* **55**(6), 1965–1975 (2012).
7. W. R. Zipfel et al., "Live tissue intrinsic emission microscopy using multiphoton-excited native fluorescence and second harmonic generation," *Proc. Natl. Acad. Sci. U. S. A.* **100**(12), 7075–7080 (2003).
8. E. Brown et al., "Dynamic imaging of collagen and its modulation in tumors in vivo using second-harmonic generation," *Nat. Med.* **9**(6), 796–800 (2003).
9. F. Ganikhanov et al., "High-sensitivity vibrational imaging with frequency modulation coherent anti-Stokes Raman scattering (FM CARS) microscopy," *Opt. Lett.* **31**(12), 1872–1874 (2006).
10. H. Kano, "Molecular vibrational imaging of a human cell by multiplex coherent anti-Stokes Raman scattering microspectroscopy using a supercontinuum light source," *J. Raman Spectrosc.* **39**(11), 1649–1652 (2008).
11. J. Imitola et al., "Multimodal coherent anti-Stokes Raman scattering microscopy reveals microglia-associated myelin and axonal dysfunction in multiple sclerosis-like lesions in mice," *J. Biomed. Opt.* **16**(2), 021109 (2011).
12. D. Li et al., "In vivo and simultaneous multimodal imaging: integrated multiplex coherent anti-Stokes Raman scattering and two-photon microscopy," *Appl. Phys. Lett.* **97**(22), 223702 (2010).
13. C. Brackmann et al., "Nonlinear microscopy of lipid storage and fibrosis in muscle and liver tissues of mice fed high-fat diets," *J. Biomed. Opt.* **15**(6), 066008 (2010).
14. J. Lin et al., "Assessment of liver steatosis and fibrosis in rats using integrated coherent anti-Stokes Raman scattering and multiphoton imaging technique," *J. Biomed. Opt.* **16**(11), 116024 (2011).
15. D. S. Choi et al., "High-speed imaging of broadband multiplex coherent anti-Stokes Raman scattering microscopy using a supercontinuum source," *Jpn. J. Appl. Phys.* **50**(2), 022401 (2011).
16. J. H. Lee et al., "Comparative study of breast normal and cancer cells using coherent anti-Stokes Raman scattering microspectroscopy imaging," *Appl. Phys. Express* **5**(8), 082401 (2012).
17. H. Barash et al., "Functional magnetic resonance imaging monitoring of pathological changes in rodent livers during hyperoxia and hypercapnia," *Hepatology* **48**(4), 1232–1241 (2008).
18. G. Gomori, "A rapid one-step trichrome stain," *Am. J. Clin. Pathol.* **20**(7), 661–664 (1950).
19. G. Poli, E. Albano, and M. U. Dianzani, "The role of lipid peroxidation in liver damage," *Chem. Phys. Lipids* **45**(2–4), 117–142 (1987).
20. P. Bedossa et al., "Deposition and remodelling of elastic fibres in chronic hepatitis," *Virchows Arch. A: Pathol. Anat. Histopathol.* **417**(2), 159–162 (1990).